European Journal of Mechanics A/Solids 47 (2014) 246–253

Contents lists available at ScienceDirect

European Journal of Mechanics A/Solids

journal homepage: www.elsevier.com/locate/ejmsol

Directional adhesion of gecko-inspired two-level fibrillar structures

L.W. He [a, b], S.P. Yan [c], J.R. Chu [b, *]

[a] Changchun Institute of Optics, Fine Mechanics and Physics, Chinese Academy of Sciences, Changchun 130021, PR China
[b] Department of Precision Machinery and Precision Instrumentation, School of Engineering Science, University of Science and Technology of China, Hefei 230036, PR China
[c] Institute of Structural Mechanics, China Academy of Engineering Physics, Mianyang, Sichuan 621900, PR China

ARTICLE INFO

Article history:
Received 21 January 2013
Accepted 2 May 2014
Available online 10 May 2014

Keywords:
Gecko-inspired adhesives
Adhesion mechanics
Normal pull-off force

ABSTRACT

Recently gecko's feet and gecko-inspired two-level fibrillar adhesives have been found to show directional adhesion property. In this paper, a theoretical model is proposed to predict the directional adhesion law of a two-level seta. The model predicts that for a typical two-level seta, there exists a structural parameters-dependent critical shear force, below and above which the bending deformation dominates or the axial deformation dominates. In the bending deformation dominated region, the adhesion force increases almost linearly with the applied shear force and the adhesion law can be tuned effectively by varying the structural parameters; while in the axial deformation dominated region, the adhesion force is no longer limited by the bending deformation and the adhesion law is almost the same with that predicted by the classical Kendall model. Additionally, an approximately optimum structure behaving consistently with geckos' hierarchical setal arrays is obtained by designing the structural parameters properly, especially the slanted angles. Thus this model can aid in interpreting the experimental test outcomes and designing optimal biomimetic two-level adhesives.

1. Introduction

Distinctive hairy attachment systems of geckos have extraordinary controllable adhesive abilities on vertical walls and ceilings. These systems consist of array of tilted setae with two or more levels of hierarchy, which allow for a large contact area on almost any surface and hence feature high adhesion and friction mainly derived from molecular interaction (Autumn et al., 2000; Autumn et al., 2002). The topmost level of seta, which directly contacts with or peels from the substrate during the locomotion, appears as one thin-film terminal element of spatulate shape and is also called spatula.

The asymmetrical or tilted adhesive structure of the seta endows gecko's feet the directional adhesion property, and thus enables geckos to achieve strong attachment and to detach easily in a controllable manner (Autumn et al., 2006). Specifically speaking, a gecko gains strong adhesion strength when it applies a shear force along the griping direction on the substrate; but when it retracts the shear force or applies the shear force along the opposite direction, the adhesion strength vanishes and the topmost spatula peels easily from the substrate. This phenomenon arouses lots of research interests in exploring its mechanism (Chen et al., 2009, 2008; Filippov et al., 2011; Gao et al., 2005; Peng et al., 2010; Pesika et al., 2007; Tian et al., 2006; Varenberg et al., 2010; Yao, 2013; Yao and Gao, 2006, 2009), and also stimulates extensive developments of biomimetic single-level (Aksak et al., 2007; Lee et al., 2008) and hierarchical fibrillar adhesives (Jeong et al., 2009; Jin et al., 2012; Murphy et al., 2009) as well as applications of directional adhesion in robots (Yu et al., 2011) and transfer printing (Carlson et al., 2011).

Many models have been proposed to explain the directional adhesion property of geckos and gecko-inspired fibrillar adhesives. Tian et al. (2006) proposed a frictional adhesion model based on force equilibrium and found that the peel-off force varies strongly with the peeling angle. Pesika et al. (2007) considered a length term in their peel zone model and derived a relation between the peel-off force and the peeling angle. However they did not strictly treat the deformation of the seta. Peng et al. (2010) studied the effect of the contact length of a nanofilm on the adhesion force. Gao et al. (2005) simulated the adhesion behavior of a curved seta and found that the adhesion force is maximized when the pulling angle is about 30°. Based on this study, Yao and Gao (2006) further studied the amplifying effect of gecko's hierarchical structure on its directional adhesion property. Chen et al. (2008) proposed a hierarchical model to concisely explain the adhesion behavior by modeling the spatula level, the seta level and the toe level as a peeling film described by the Kendall model, a stretchable rod and an elastic plate under displacement controlled pulling respectively.

* Corresponding author.
E-mail address: jrchu@ustc.edu.cn (J. Chu).

http://dx.doi.org/10.1016/j.euromechsol.2014.05.001
0997-7538/

However most of these works only model the bottom level of the seta (Gao et al., 2005) or the topmost spatula (Chen et al., 2009; Filippov et al., 2011; Peng et al., 2010; Pesika et al., 2007; Varenberg et al., 2010) or treat them separately (Chen et al., 2008; Tian et al., 2006). Numerical models such as FEM models (Sauer, 2009) could treat the two levels simultaneously, but they could not be easily utilized for exploring the correlation between the structure and the corresponding adhesion property and optimizing structural parameters. Particularly, it is not clearly known how the two-level structure of geckos' feet and gecko-inspired adhesives contributes to the distinctive directional adhesion property as geckos show in a directional adhesion test. Motivated by such a problem, we propose a theoretical model that can predict the directional adhesion behavior of a two-level fibrillar structure.

2. Modeling

A two-level seta is considered as shown in Fig. 1(c). The bottom level is a beam with length l_1, bending stiffness EI_1, and axial stiffness EA_1, and the top level is a spatula with length l_2, bending stiffness EI_2, and axial stiffness EA_2. The slanted angle of the beam at the bottom is α_1, and the angle between the beam and the spatula is α_2. The latter angle is prevalent in bio-/biomimetic adhesives as shown in Fig. 1(a) and (b) (Arzt et al., 2003; Filippov et al., 2011) and is found to have a significant influence on the adhesion properties as will be shown in this paper. The adhesion between the two-level seta and a rigid contacting surface under the coupling effect of a normal force F_n and a shear force F_t is studied in the present paper. The work of adhesion per unit length of the contact interface between them is denoted by ω. When being applied a comparatively large F_n and F_t, the seta will deform and form side contact with the rigid surface. The arc length of the non-contact part along the whole structure, *i.e.* the arc-length coordinate s' of the contact boundary, is termed the real "non-contact length" a'. The slanted angles of the beam and spatula after deformation are termed θ_1 and θ_2 as shown in Fig. 1(d).

A side contact model for a single-level extensible fiber was proposed in a previous paper (He et al., 2013). In the paper we applied a variational method to the total energy of the system consisting of the axial strain energy, the bending strain energy, the interface energy and the potential energy of external forces. By formulating the energy functional in a convected coordinate s which is initially established along the arc length of the undeformed fiber, we derived the governing equation and adhesion boundary condition for the fiber so that the adhesion mechanics problem of an extensible fiber can be tackled in a very concise way. The governing equation and adhesion boundary condition will be directly cited for modeling the two-level seta in the present paper.

Applying the governing equation to the beam and the spatula respectively, we have:

$$EI_1\frac{d^2\theta_1}{ds^2}+(F_n\sin\theta_1+F_t\cos\theta_1)[1+(F_t\sin\theta_1-F_n\cos\theta_1)/EA_1]=0,\quad 0\le s\le l_1, \tag{1}$$

$$EI_2\frac{d^2\theta_2}{ds^2}+(F_n\sin\theta_2+F_t\cos\theta_2)[1+(F_t\sin\theta_2-F_n\cos\theta_2)/EA_2]=0,\quad l_1\le s\le a. \tag{2}$$

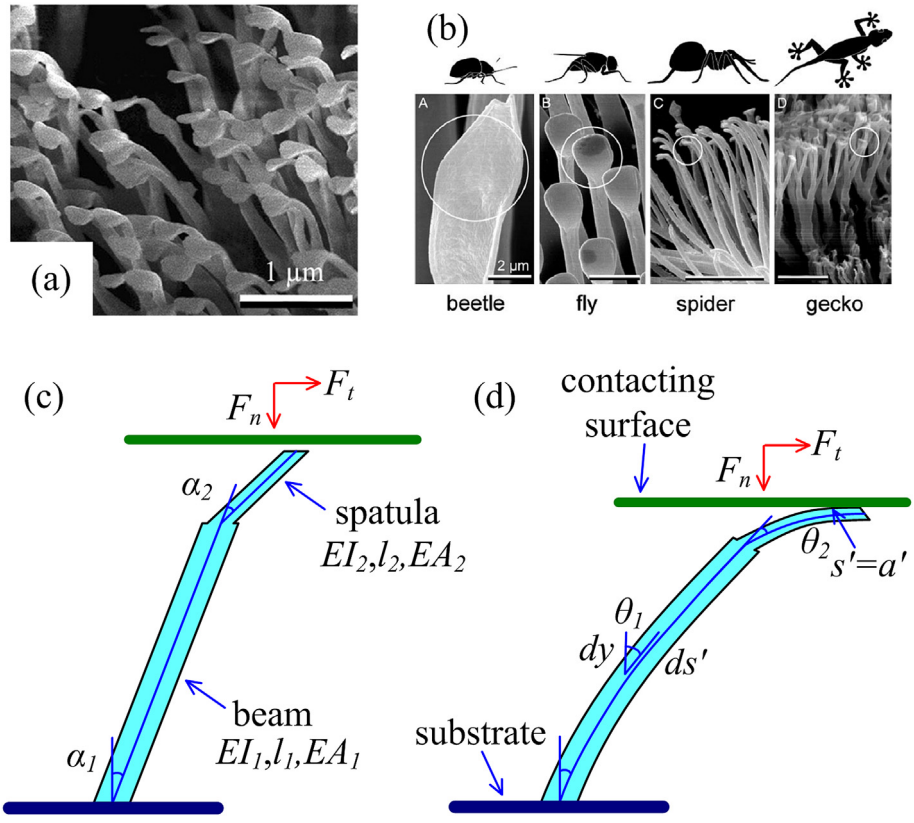

Fig. 1. SEM pictures of biological adhesives and schematic figures of a two-level fibrillar structure. (a) Spatulae of Gekko gecko (Filippov et al., 2011); (b) feet structures of typical animals with adhesion capabilities (Arzt et al., 2003, Copyright (2003) National Academy of Sciences, U.S.A.); (c) and (d) the undeformed and deformed configurations of the two-level seta.

where θ_1 and θ_2 are the slanted angles of the beam and the spatula at the convected coordinate s, and a is the non-contact length measured in the convected coordinate. In the following analysis, a is called the non-contact length for simplicity. As has been shown in the previous paper (He et al., 2013), small axial strain and negligible shear strain are assumed during the modeling process, but it should also be noted that axial deformation and large bending deformation are captured in the above governing equations. Especially when the axial stiffness EA_i ($i = 1,2$) is infinite, *i.e.* neglecting the axial deformation, the governing equations degenerate to the classical deformation equation of beam with large bending deformation.

Applying the adhesion boundary condition to the two-level seta yields:

$$\left[\frac{1}{2}EI_2\left(\frac{d\theta_2}{ds}\right)^2+\frac{(F_t\sin\theta_2-F_n\cos\theta_2)^2}{2EA_2}\right]_{s=a}=\omega. \tag{3}$$

From the point of view of fracture mechanics, Eq. (3) means that at equilibrium, the energy release rate of the system (can be seen as an interfacial crack) equals the work of adhesion.

By using the angle relation and bending moment condition at the connecting point between the beam and the spatula, we have:

$$\theta_2(l_1)-\theta_1(l_1)=\alpha_2,\quad EI_2\frac{d\theta_2}{ds}(l_1)=EI_1\frac{d\theta_1}{ds}(l_1). \tag{4}$$

The essential boundary conditions can also be written as:

$$\theta(0)=\alpha_1,\quad \theta(a)=\frac{\pi}{2}. \tag{5}$$

The governing Eqs. (1) and (2) and the adhesion boundary condition (3) show that both the large bending deformation and the axial deformation bring geometrical nonlinearity to the adhesion problem.

For a special but insightful case of no external forces being applied to the two-level seta, Eqs. (1) and (2) degenerate to, $EI_1 d^2\theta_1/ds^2 = 0$, $0 \le s \le l_1$, $EI_2 d^2\theta_2/ds^2 = 0$, $l_1 \le s \le a$, *i.e.* $EI_1 d\theta_1/ds = EI_2 d\theta_2/ds$ = constant bending moment, where the Eq. (4) is utilized. This means that the seta undergoes a pure bending deformation. Meanwhile Eq. (3) degenerates to $[1/2EI_2(d\theta_2/ds)^2]_{s=a} = \omega$, *i.e.* $EI_2(d\theta_2/ds)_{s=a} = \sqrt{2EI_2\omega}$, which implies that the equivalent bending moment induced by the adhesion force at the adhesion boundary is $M_{eq} = \sqrt{2EI_2\omega}$. Assuming that there exists a finite contact length l_c ($l_c = l - a$) between the seta and the rigid surface, the bending angles for the beam and the spatula are $M_{eq}l_1/EI_1$ and $M_{eq}(l_2 - l_c)/EI_2$ respectively. By using Eqs. (4) and (5), we obtain

$$\frac{M_{eq}(l_2-l_c)}{EI_2}+\frac{M_{eq}l_1}{EI_1}=\frac{\pi}{2}-(\alpha_1+\alpha_2). \tag{6}$$

This equation can be written in the following non-dimensional form:

$$\left(1-\bar{l}_c\right)=\left(\frac{l_2}{l_1}\right)^{-1}\left(\frac{EI_2}{EI_1}\right)^{1/2}\left\{\sqrt{\frac{EI_1}{2\omega l_1^2}}\left[\frac{\pi}{2}-(\alpha_1+\alpha_2)\right]-\left(\frac{EI_2}{EI_1}\right)^{1/2}\right\}, \tag{7}$$

where $\bar{l}_c = l_c/l_2$. Only when $\sqrt{EI_1/(2\omega l_1^2)}$ is small enough, l_2/l_1 is large enough, and the slanted angles α_1 and α_2 are large enough that the right hand side of Eq. (7) is smaller than 1, there could exist a finite contact length. Moreover, the right hand side of Eq. (7) varies non-monotonically with EI_2/EI_1 and the turning point is $\sqrt{EI_1/2\omega l_1^2}(\pi/4 - \alpha_1 + \alpha_2/2)$. This is mainly due to a significant fact that the equivalent bending moment is proportional to the square root of EI_2. For a single-level structure, the contact length also increases with the decrease of $\sqrt{EI/(2\omega l^2)}$, where EI and l are the bending stiffness and length of the single-level structure.

For the general case, the adhesion problem can be analyzed as follows. Firstly Eqs. (1) and (2) can be integrated to take the following forms respectively:

$$\frac{1}{2}EI_1\left(\frac{d\theta_1}{ds}\right)^2=-F_t\sin\theta_1+F_n\cos\theta_1-\frac{(F_t\sin\theta_1-F_n\cos\theta_1)^2}{2EA_1}+M', \tag{8}$$

$$\frac{1}{2}EI_2\left(\frac{d\theta_2}{ds}\right)^2=-F_t\sin\theta_2+F_n\cos\theta_2-\frac{(F_t\sin\theta_2-F_n\cos\theta_2)^2}{2EA_2}+M, \tag{9}$$

where M' and M are integration constants to be determined. By applying an appropriate variable transformation to Eq. (9) as has been shown in the previous paper (He et al., 2013), we can obtain a formula as shown below:

$$\frac{\sqrt{2EI_2}}{\sqrt{M(1+q-p)(1+\lambda_2)}}[F(\varphi(\pi/2),m)-F(\varphi(\theta_2(l_1)),m)]=a-l_1, \tag{10}$$

where $F(x, m)$ is the incomplete elliptical integral of the first kind, and

$$M=F_t+\omega,\ N=\sqrt{F_n^2+F_t^2},\ \tan\phi=\frac{F_n}{F_t},\ q=\frac{N}{M},\ p=\frac{N^2}{2EA_2M},$$
$$\lambda_1=\frac{(q-2p)+\sqrt{q^2+4p}}{1+q-p},\ \lambda_2=\frac{-(q-2p)+\sqrt{q^2+4p}}{1+q-p},\ m=\frac{\lambda_1+\lambda_2}{1+\lambda_2},$$
$$\varphi(\theta)=\begin{cases}\mathrm{Arcsin}\left[\sqrt{\dfrac{(1+\lambda_2)(1+\sin(\theta-\phi))}{2+\lambda_2(1+\sin(\theta-\phi))}}\right], & \theta-\phi\le\dfrac{\pi}{2}\\ \pi-\mathrm{Arcsin}\left[\sqrt{\dfrac{(1+\lambda_2)(1+\sin(\theta-\phi))}{2+\lambda_2(1+\sin(\theta-\phi))}}\right], & \theta-\phi>\dfrac{\pi}{2}\end{cases}. \tag{11}$$

Based on Eq. (8), Eq. (9) and the boundary condition (Eq. (4)) at $s = l_1$, we have:

$$M'=\frac{EI_2}{EI_1}\left(N\sin(\phi-\theta_2(l_1))-\frac{1}{2}\frac{N^2}{EA_2}\sin^2(\phi-\theta_2(l_1))+M\right)$$
$$-N\sin(\phi-\theta_2(l_1)+\alpha_2)+\frac{1}{2}\frac{N^2}{EA_1}\sin^2(\phi-\theta_2(l_1)+\alpha_2). \tag{12}$$

Therefore via applying a similar variable transformation to Eq. (8), we obtain another formula as shown below:

$$\frac{\sqrt{2EI_1}}{\sqrt{M'(1+q'-p')(1+\lambda_2')}}[F(\varphi'(\theta_2(l_1)-\alpha_2),m')-F(\varphi'(\alpha_1),m')]=l_1, \tag{13}$$

where

$$q' = N/M',\ \ p' = N^2/(2EA_1M'),$$

$$\lambda_1' = \frac{(q'-2p') + \sqrt{q^2+4p'}}{1+q'-p'},\ \ \lambda_2' = \frac{-(q'-2p') + \sqrt{q'^2+4p'}}{1+q'-p'},$$

$$m' = \frac{\lambda_1' + \lambda_2'}{1+\lambda_1'},$$

$$\varphi'(\theta) = \begin{cases} \mathrm{Arcsin}\left[\sqrt{\dfrac{(1+\lambda_2')(1+\sin(\theta-\phi))}{2+\lambda_2'(1+\sin(\theta-\phi))}}\right], & \theta-\phi \le \dfrac{\pi}{2} \\ \pi - \mathrm{Arcsin}\left[\sqrt{\dfrac{(1+\lambda_2')(1+\sin(\theta-\phi))}{2+\lambda_2'(1+\sin(\theta-\phi))}}\right], & \theta-\phi > \dfrac{\pi}{2} \end{cases} \tag{14}$$

By combing Eqs. (10) and (13), a group of equations describing the mechanical response of the two-level seta is obtained as shown below:

$$\begin{cases} \dfrac{\sqrt{2EI_2}}{\sqrt{M(1+q-p)(1+\lambda_2)}}[F(\varphi(\pi/2),m) - F(\varphi(\theta_2(l_1)),m)] = a - l_1 \\ \dfrac{\sqrt{2EI_1}}{\sqrt{M'(1+q'-p')(1+\lambda_2')}}[F(\varphi'(\theta_2(l_1)-\alpha_2),m') - F(\varphi'(\alpha_1),m')] = l_1 \end{cases} \tag{15}$$

The following conclusions can be made based on Eq. (15). On one hand, if the applied forces F_t and F_n is given, $\theta_2(l_1)$ can be firstly solved from the second Equation of Eq. (15) and then a can be found from the first Equation. On the other hand, it can be assumed that the two-level seta loses side contact when $a = l_1 + l_2$ (The jumping-off mode of losing sie contact is not considered here, for it is possible for a positive F_t only when $\sqrt{EI_1/(2\omega l_1^2)}$ is small enough, l_2/l_1 is large enough, or the slanted angles α_1 andα_2 are very large). This is similar to that discussed for the single-level one in our previous papers (He et al., 2012, 2013), therefore by setting $a = l_1 + l_2$ and finding the roots (F_n and $\theta_2(l_1)$) of the implicit Eq. (15) for each given F_t, a critical line of adhesion (contours of $a = l_1 + l_2$) in a 2D force space $F_n - F_t$ can be easily obtained as displayed in Fig. 2. The critical line of adhesion means that for a given F_t, once the applied normal force F_n is decreased to reach the critical F_n at the critical line, the seta will lose side contact with the contacting surface. If the critical F_n on a critical line for a given F_t is negative, its absolute value is termed the "normal pull-off force" ($(F_n)_{pull\text{-}off}$) or the normal adhesion force and detachment will happen. We will discuss the results in the following section.

3. Results and discussions

Set $EI_1/\omega l_1^2 = 5$, $\alpha_1 = \pi/6$,$\alpha_2 = \pi/6$, $EI_2/EI_1 = 0.4$, $l_2/l_1 = 0.1$, $EA_2/\omega = 50$ and $EA_1/\omega = \infty$ as reference variables. By changing one variable at a time, the directional adhesion behavior of the two-level seta is studied systematically. The non-dimensional normal and shear forces are denoted by$\overline{F}_n = F_n/\omega$ and $\overline{F}_t = F_t/\omega$.

3.1. General description of the directional adhesion behavior

Figs. 2 and 3 show that the critical line of adhesion for the two-level seta usually consists of two different parts. At the lower part, $(F_n)_{pull\text{-}off}$ is smaller than the critical value determined by the Kendall model (Kendall, 1975) (a classical model used to predict the peeling force of an extensible film from a rigid substrate without considering the bending deformation) and increases almost linearly with F_t. While at the upper part, F_n changes with F_t almost along the critical line of adhesion for the Kendall model. This is because at the lower part, increasing the shear force within a certain degree benefits for closing the interfacial crack to a larger extent (increasing the contact length), hence a higher normal pull force is needed to completely open the crack. While when F_t is close to the maximum allowable shear force $(F_t)_{\max}$ ($(F_t)_{\max} = \sqrt{2EA_2\omega}$), the axial deformation energy per unit length at the contact boundary, which is a quadratic function of F_t, dominates the energy release rate as shown in the left hand side of Eq. (3). Thus in this case F_t contributes to the opening of the interfacial crack and the adhesion force decreases with the increase of F_t. Therefore the 2D force space can be roughly divided into a bending deformation dominated region (small F_t relative to $(F_t)_{\max}$) and an axial deformation dominated region (large F_t close to $(F_t)_{\max}$), so that the lower part belongs to the bending deformation dominated region and the upper part belongs to the axial deformation dominated region.

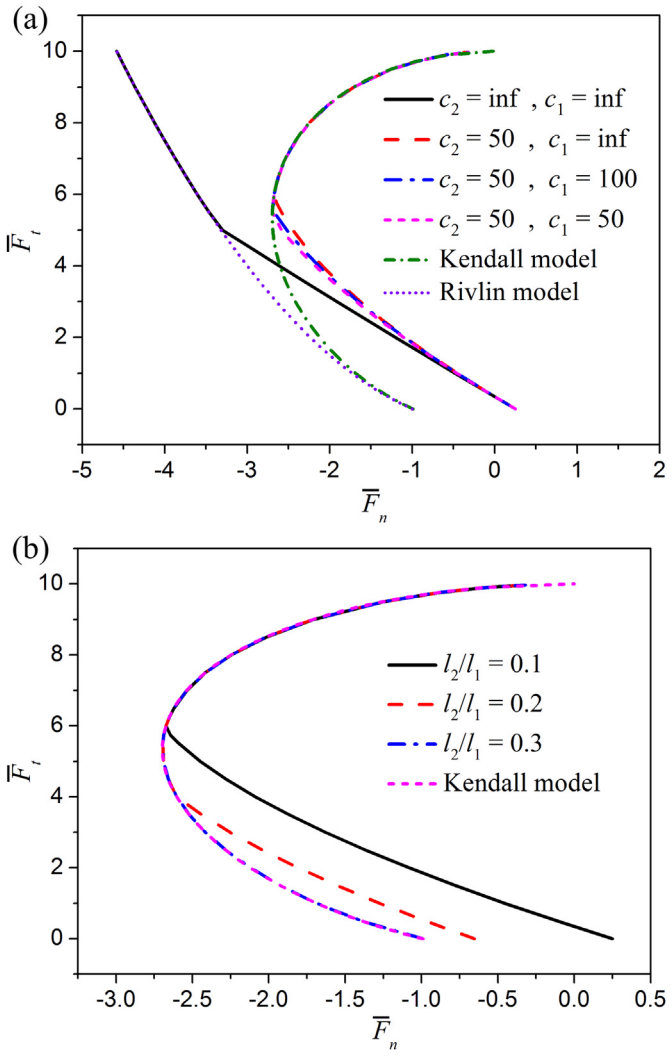

Fig. 2. Effects of the axial stiffness (a) and the length ratio l_2/l_1 (b) on the critical line of adhesion for the two-level seta. In (a), $c_2 = EA_2/\omega$, $c_1 = EA_1/\omega$ and the "inf" denotes infinite.

Corresponding to the above observations, the directional adhesion behavior for typical structures can be approximately described quantitatively. Firstly in the bending deformation dominated region, the equation for the critical line can be approximated as:

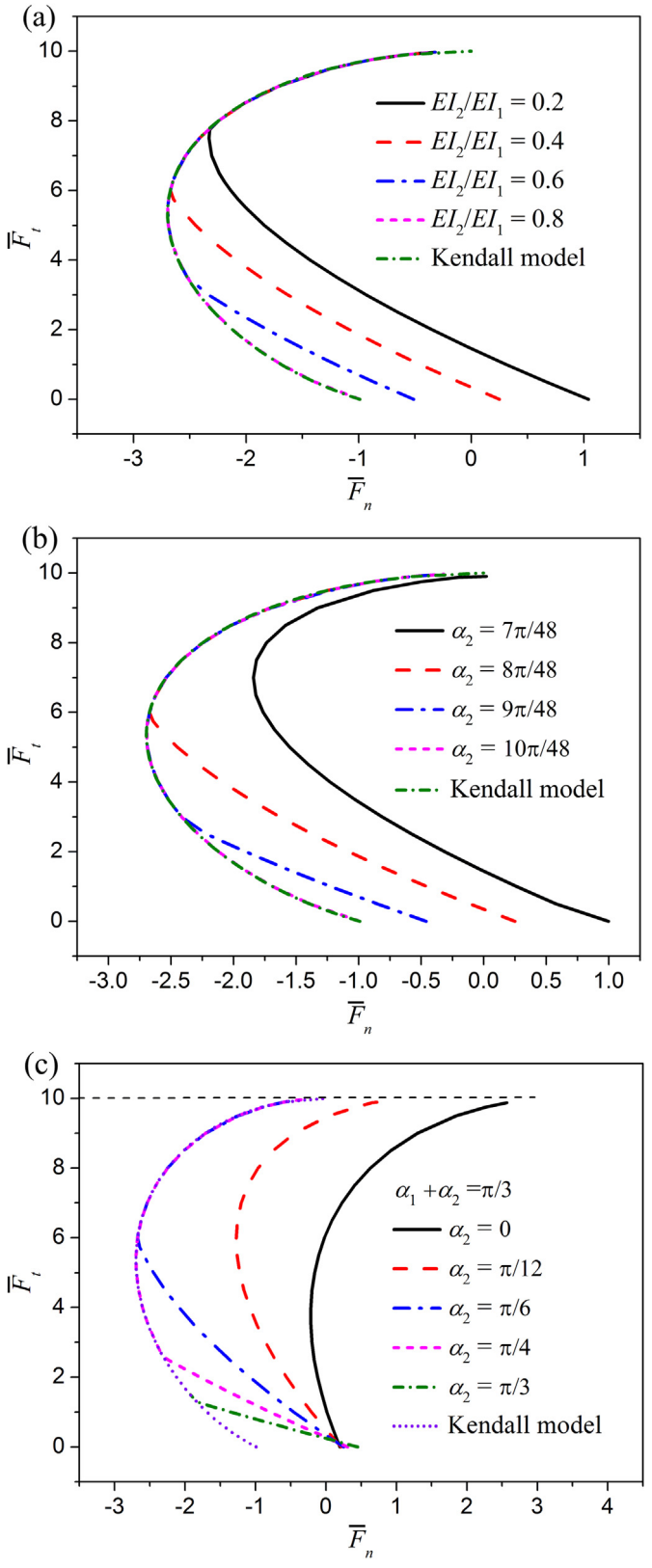

Fig. 3. Effects of the bending stiffness ratio (a), the second slanted angle (b) and the distribution of the two angles (c) on the critical line of adhesion for the two-level seta.

$$F_n = (F_n)_0 + \frac{F_t}{k}, \tag{16}$$

where k is the slope of the straight line as shown in Fig. 2 and $(F_n)_0$ means the adhesion force of the structure in its natural state ($F_t = 0$). It is clear that $1/|k|$ characterizes the increasing rate of the normal adhesion force with the applied shear force. In the axial deformation dominated region, the equation for the critical line is usually the same with that of the Kendall model (Kendall, 1975), which is also given below:

$$\sqrt{F_t^2 + F_n^2} + \frac{F_t^2 + F_n^2}{2EA_2} - F_t - \omega = 0. \tag{17}$$

The maximum $(F_n)_{pull\text{-}off}$ is another important characteristic parameter for the directional adhesion behavior. It increases with the axial stiffness of the spatula.

The effect of the axial stiffness of the seta on the adhesion behavior is displayed in Fig. 2(a). If the axial deformation is not considered ($c_1 = c_2 = \infty$), $(F_n)_{pull\text{-}off}$ increases monotonically with F_t along the critical line for the Rivlin model (Rivlin, 1944) at the upper part of the critical line, different from the extensible case ($c_1 = c_2 = 50$). Fig. 2(a) also shows that the differences among curves for the cases of ($c_2 = 50$, $c_1 = 50$), ($c_2 = 50$, $c_1 = 100$) and ($c_2 = 50$, $c_1 = \infty$) are relatively small and negligible, from which it can be inferred that the axial stiffness of the beam has almost negligible influence on the adhesion behavior. Therefore the existence of a maximum $(F_n)_{pull\text{-}off}$ is due to the extensibility of the topmost spatula, and in the following analysis, the axial stiffness of the beam is taken to be infinite as mentioned in the beginning of this section.

The effects of the length ratio, the bending stiffness ratio, and the second slanted angle of the two-level seta on the directional adhesion behavior are also studied. Figs. 2(b), 3(a) and (b) show respectively that in the bending deformation dominated region, if the applied shear force F_t is fixed, the normal adhesion force increases with the increase of l_2/l_1 and EI_2/EI_1 in the range of $EI_2/EI_1 > 0.2$ and also increases with the increase of the slanted angle α_2. These results can be explained qualitatively as follows. Under the effect of the same normal and shear forces within the bending deformation dominated region, structure with larger l_2/l_1, larger EI_2/EI_1 (which should be beyond the turning point) or larger slanted angles can form larger contact length with the contacting surface as has been demonstrated for the case of no external forces being applied in Section.2 (in that case the turning point for EI_2/EI_1 is about 0.17), thus a larger normal pull-off force is usually required to completely peel the structure from the surface. While Figs. 2(b), 3(a) and (b) also show that, in the axial deformation dominated region the adhesion force is usually saturated and does not rely on these structural parameters, for bending deformation is accommodated and no longer limits the normal pull-off force.

A significant difference of the adhesion behavior of a two-level seta from that of a single-level is shown in Fig. 4. For a single level setae, if the non-dimensional stiffness $EI/(\omega l^2)$ is much smaller than 1, its critical line of adhesion could be very close to the Kendall limit (eg. the case of $EI/\omega l^2 = 1/2$ shown in Fig. 4), but meanwhile its normal adhesion force in its natural state ($F_t = 0$) is comparatively large and cannot be decreased by adjusting its slanted angle (He et al., 2013). But for the two level setae, if the structural parameters are within a certain range, the $(F_n)_0$ can be independently controlled and meanwhile the maximum normal pull off force remains constant as demonstrated in Figs. 2(b), 3(a) and (b). This is because for a typical two-level setae, in the bending deformation dominated region, the bending deformation limits the adhesion

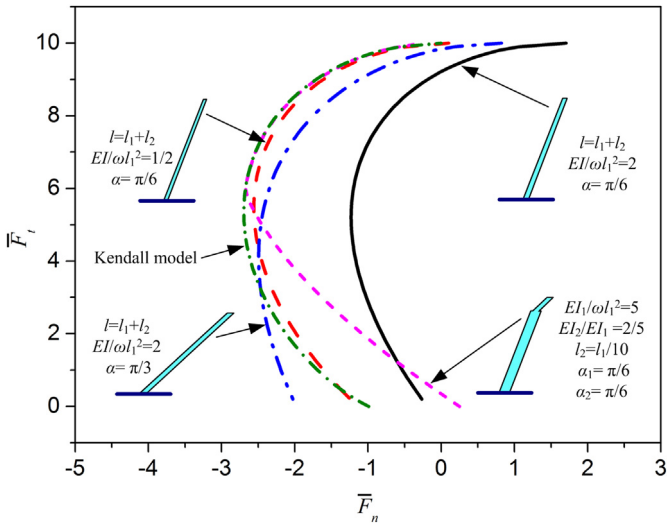

Fig. 4. Comparison of the directional adhesion behavior of the two-level seta with single-level ones (for all the structures, $EA/\omega = 50$or $EA_2/\omega = 50$).

force and the adhesion force can be adjusted by many variables; but in the axial deformation dominated region, the bending deformation is accommodated, so that the normal pull off force saturates to the limit set by the Kendall model.

3.2. Tunability of the directional adhesion property

With the purpose of tuning the directional adhesion property of the seta, the influences of the structural parameters on the slope k and the adhesion force $(F_n)_0$ of the critical line are further discussed. The results show that decreasing $EI_1/\omega l_1^2$, or increasing α_1, α_2 or l_2/l_1 leads to effective reduction of $(F_n)_0$, i.e. enhancing the adhesion performance, but $(F_n)_0$ does not decrease monotonically with EI_2/EI_1. It is also revealed that only l_2/l_1 and α_2 have an observable influence on the slope k. A case of changing α_2 while keeping $\alpha_1+\alpha_2$ constant is further analyzed. Fig. 3(c) demonstrates that the $(F_n)_0$ almost remains constant, while the slope could be adjusted effectively by distributing the two angles.

In order to interpret these results, the small deformation theory is adopted to derive two simple formulas to show the effects of the structural parameters on the characteristic parameters k and $(F_n)_0$. Although they are not quantitatively correct, they could help interpret the directional adhesion results qualitatively. In the bending deformation dominated region, the axial deformation is neglected for its influences on $(F_n)_0$ and k are comparatively small. Because we just care about the critical state of adhesion, only the case of $a = l_1 + l_2$ is considered. By using the fundamental theory of mechanics of materials, we have:

$$\frac{[F_t\cos(\alpha_1+\alpha_2)+F_n\sin(\alpha_1+\alpha_2)]l_2^2}{2EI_2}+\frac{M_{eq}l_2}{EI_2}+\frac{[F_t\cos\alpha_1+F_n\sin\alpha_1]l_1^2}{2EI_1}+\frac{[F_t\cos(\alpha_1+\alpha_2)l_2+F_n\sin(\alpha_1+\alpha_2)l_2+M_{eq}]l_1}{EI_1}=\frac{\pi}{2}-(\alpha_1+\alpha_2), \tag{18}$$

where $M_{eq}=\sqrt{2EI_2\omega}$.

Let $F_t = 0$ in Eq. (18), then the following formula can be obtained:

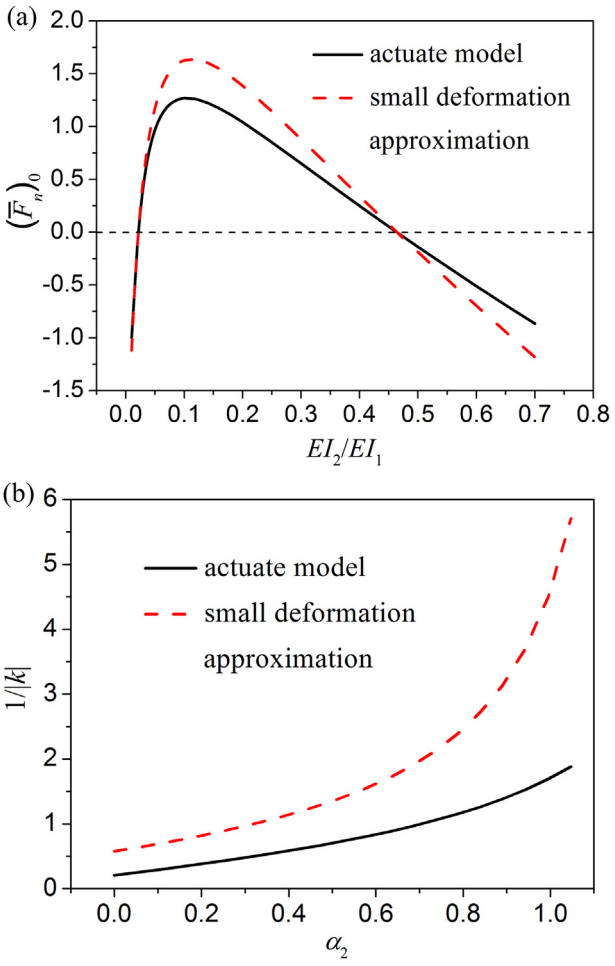

Fig. 5. (a) Effect of the bending stiffness ratio on the adhesion force in its natural state $(F_n)_0$ and (b) effect of the slanted angle α_2 on the increasing rate $1/|k|$ of the adhesion force with the applied shear force ($\alpha_1+\alpha_2=\pi/6$).

$$(\overline{F}_n)_0=\frac{(F_n)_0}{\omega}=\frac{\sqrt{8\mu}}{\sin(\alpha_1+\alpha_2)}\frac{\sqrt{\mu/2}\Delta\theta-\xi^{1/2}-x\xi^{-1/2}}{x^2/\xi+2x+\sin\alpha_1/\sin(\alpha_1+\alpha_2)}, \tag{19}$$

where $\Delta\theta=\pi/2-(\alpha_1+\alpha_2)$, $\mu=EI_1/\omega l_1^2$, $\xi=EI_2/EI_1$,$x=l_2/l_1$. By using Eq. (7), Eq. (19) can be reduced to the following form.

$$(\overline{F}_n)_0=\frac{\sqrt{8\mu}}{\sin(\alpha_1+\alpha_2)\left[x^2/\xi+2x+\sin\alpha_1/\sin(\alpha_1+\alpha_2)\right]}\frac{1}{\xi^{1/2}}\left(-\frac{l_c}{l_1}\right). \tag{20}$$

From Eq. (20), it can be inferred that if the structure could hold the adhesion state ($l_c > 0$) only under the action of the equivalent bending moment M_{eq}, it has adhesion capability in its natural state ($F_t = 0$); otherwise if l_c does not exist or $l_c < 0$, we have $(F_n)_0 > 0$, which means that the structure is not sticky in the natural state, thus behaving like gecko's feet. In fact, it is natural to draw this conclusion, and it does not rely on the small deformation approximation. The $(\overline{F}_n)_0-\xi$ curves obtained from the small deformation approximation (Eq. (19)) and the actuate model are plotted as shown in the Fig. 5 (a). It shows that they are in good agreement with each other qualitatively, and both the two peak positions of the two curves are also very close to the approximate value $x = 0.1$.

By differentiating Eq. (18), the absolute value of the slope k can as be obtained as:

$$|k| = \frac{|F_t|}{|F_n|} \approx \left|\frac{\partial F_t}{\partial F_n}\right| = \tan(\alpha_1+\alpha_2)\left[1 - \frac{1}{\sin^2(\alpha_1+\alpha_2)\left[\left(\frac{x^2/\xi+2x}{\sin\alpha_2}+\cot\alpha_2\right)\cot(\alpha_1+\alpha_2)+1\right]}\right] \tag{21}$$

From this formula we can see that μ does not affect the slope, and if $x \ll 2\xi$, the influence of ξ is negligible. It could be checked that only x and α_2 have a noticeable effect on the slope. When $\alpha_1+\alpha_2$ remains constant, increasing α_2 can significantly increase $1/|k|$. The $1/|k| - \alpha_2$ curves calculated from the approximation and the actuate model are displayed in Fig. 5(b), which shows that they are qualitatively consistent with each other. Therefore it can be summarized that the two formulas derived from the small deformation approximation could help interpret the tunability of the directional adhesion law and designing structural parameters.

From the point of view of optimization, it should be guaranteed that the hierarchical structure does not have adhesion capability in its natural state, i.e.$(F_n)_0 \geq 0$, so that no work needs to be done to break up the adhesion. In order to achieve detachment, it is only necessary to decrease F_t to some extent. According to the above discussion, such a relation

$$\left(\frac{l_2}{l_1}\right)^{-1}\left(\frac{EI_2}{EI_1}\right)^{1/2}\left\{\sqrt{\frac{EI_1}{2\omega l_1^2}}\left[\frac{\pi}{2}-(\alpha_1+\alpha_2)\right]-\left(\frac{EI_2}{EI_1}\right)^{1/2}\right\} \geq 1 \tag{22}$$

can be applied to ensure that $(F_n)_0 \geq 0$. Therefore in order to optimize the structure, balance should be made among the following parameters: $EI_1/\omega l_1^2$,EI_2/EI_1, l_2/l_1 and $\alpha_1+\alpha_2$. Then the total angle $\alpha_1+\alpha_2$ should be reasonably distributed between $\alpha_1$and α_2. In one opposite case of α_2 being very large and α_1 being almost zero, the normal stiffness of the seta after the spatula forms complete contact with the contacting surface ($K_n = 3EI_1/\sin^2\alpha_1$) is too large, which is not beneficial for achieving strong adhesion on rough surfaces. On the other opposite case of very small α_2 and large α_1, the maximum $(F_n)_{pull\text{-}off}$ is far lower than that given by the Kendall model (as shown in Fig. 3(c)). Thus when choosing the optimal angle for α_2, we should first guarantee the maximum $(F_n)_{pull\text{-}off}$ is maximized, and then decrease the normal stiffness (decreasing α_2) as much as possible. For the calculated case, an approximately optimum angle for α_2 is about $\pi/6$, and an optimal angle must be at its neighborhood. The critical line of adhesion for $\pi/6$ is also plotted in Fig. 6(a), and its difference with that of the Kendall model is clearly shown. Evidently for a general case, optimal values depend on other structural parameters.

3.3. Further discussions

Concerning the optimization of hierarchical fiber arrays, the structural stability (no lateral collapse happens) requires high bending stiffness, short length and large gap between adjacent fibers. While rough surface adaptability needs low effective stiffness, which in turn requires low bending stiffness, long length and large

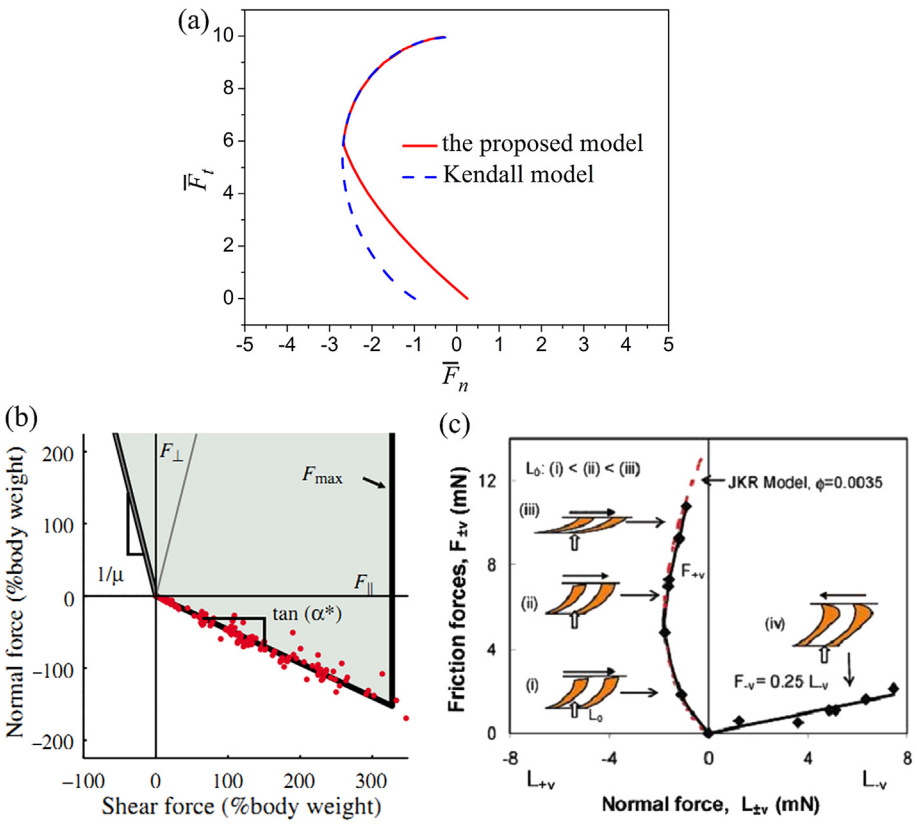

Fig. 6. Comparison of the predicted adhesion behavior for an optimal structure (a) with experimental results on gecko's feet obtained (b) in force controlled mode (Autumn et al., 2006) and (c) in displacement controlled mode (Zhao et al., 2008).

gap. As the objective of optimization, high-performance adhesion necessitates dense distribution of the fiber array and strong directionality in the adhesion of a single fiber. As discussed above, various parameters significantly influence the latter one. Thus in order to search for an optimal adhesion structure, balances should be made among these constraints and the multiple objectives. Obviously, optimization of the structural parameters is not an easy task. However, further studies on the optimization should be conducted to aid the design of hierarchical adhesives.

We also compare our model with experimental outcomes of hierarchical fibrillar bio-/biomimetic structures. The comparisons reveal that our model could explain well the directional adhesion test outcomes of gecko's hierarchical setal arrays in the literatures. Autumn et al. (2006) first did the test in a force-loaded mode and found that, as shown in Fig. 6(b), the structure is not adhesive in its natural state and the adhesion force increases almost linearly with the applied shear force until the a maximum shear force is reached. As shown in Fig. 6(a), the aforementioned optimal structure ($\alpha_2 = \pi/6$) displays such directional adhesion property. In addition, the existence of the so called "maximum shear force" is due to that when such a shear force is applied, the pull force equals the maximum pull-off force and detachment will happen. Zhao et al. (2008) also did a delicate adhesion test in a displacement-loaded mode, and plotted a complete critical line of adhesion as shown in Fig. 6(c). It shows that when the shear force exceeds the above called maximum value, the adhesion force decreases with the shear force. This result is consistent with the result predicted by our model as shown in Fig. 6(a).

Murphy et al. (2009) also conducted directional adhesion test on their two-level adhesives in displacement-loaded mode, and found similar adhesion behavior with that obtained by Zhao et al. (2008), which could also be interpreted easily by using our model. Jeong et al. (2009) tested the adhesion behavior of a fiber with a small spatula and found that the results are in good agreement with the Kendall model. It can be seen as a special case of our model when the structure is very flexible. Thus our model can help interpret experimental test outcomes of hierarchical biomimetic fibrillar structures.

4. Conclusion

In conclusion, an adhesion model is proposed to predict the directional adhesion law of two-level fibrillar bio-/biomimetic structures. The model predicts that there exists a structural parameters-dependent critical shear force, below and above which the bending deformation dominates or the axial deformation dominates. In the bending deformation dominated region, the adhesion force increases almost linearly with the applied shear force and the adhesion law can be tuned effectively by varying the structural parameters; while in the axial deformation dominated region, the adhesion force is no longer limited by the bending deformation and the adhesion law is almost the same with that predicted by the classical Kendall model. It is also demonstrated through comparisons that the model agrees well with typical experimental outcomes reported in literatures, and as has been discussed preliminarily, the obtained adhesion law can contribute to biomimetic design and structural optimization of such dry adhesives. Further exploration of the optimization method is our further work.

Acknowledgments

This work is supported by the National Basic Research Program of China (973 Program, No. 2011CB302101).

References

Aksak, B., Murphy, M.P., Sitti, M., 2007. Adhesion of biologically inspired vertical and angled polymer microfiber arrays. Langmuir 23, 3322–3332.
Arzt, E., Gorb, S., Spolenak, R., 2003. From micro to nano contacts in biological attachment devices. Proc. Nat. Acad. Sci. U. S. A. 100, 10603–10606.
Autumn, K., Dittmore, A., Santos, D., Spenko, M., Cutkosky, M., 2006. Frictional adhesion: a new angle on gecko attachment. J. Exp. Biol. 209, 3569–3579.
Autumn, K., Liang, Y.A., Hsieh, S.T., Zesch, W., Chan, W.P., Kenny, T.W., Fearing, R., Full, R.J., 2000. Adhesive force of a single gecko foot-hair. Nature 405, 681–685.
Autumn, K., Sitti, M., Liang, Y.A., Peattie, A.M., Hansen, W.R., Sponberg, S., Kenny, T.W., Fearing, R., Israelachvili, J.N., 2002. Evidence for van der Waals adhesion in gecko setae. Proc. Nat. Acad. Sci. U. S. A. 99, 12252.
Carlson, A., Kim-Lee, H.J., Wu, J., Elvikis, P., Cheng, H., Kovalsky, A., Elgan, S., Yu, Q., Ferreira, P.M., Huang, Y., 2011. Shear-enhanced adhesiveless transfer printing for use in deterministic materials assembly. Appl. Phys. Lett. 98, 264104.
Chen, B., Wu, P., Gao, H., 2009. Pre-tension generates strongly reversible adhesion of a spatula pad on substrate. J. R. Soc. Interface 6, 529–537.
Chen, B., Wu, P.D., Gao, H., 2008. Hierarchical modelling of attachment and detachment mechanisms of gecko toe adhesion. Proc. R. Soc. A 464, 1639–1652.
Filippov, A., Popov, V.L., Gorb, S.N., 2011. Shear induced adhesion: contact mechanics of biological spatula-like attachment devices. J. Theor. Biol. 276, 126–131.
Gao, H.J., Wang, X., Yao, H.M., Gorb, S., Arzt, E., 2005. Mechanics of hierarchical adhesion structures of geckos. Mech. Mater. 37, 275–285.
He, L.W., Yan, S.P., Li, B.Q., Chu, J.R., 2012. Directional adhesion behavior of a single elastic fiber. J. Appl. Phys. 112, 013516.
He, L.W., Yan, S.P., Li, B.Q., Zhao, G., Chu, J.R., 2013. Adhesion model of side contact for an extensible elastic fibre. Int. J. Solids Struct. 50, 2659–2666.
Jeong, H.E., Lee, J.-K., Kim, H.N., Moon, S.H., Suh, K.Y., 2009. A nontransferring dry adhesive with hierarchical polymer nanohairs. Proc. Nat. Acad. Sci. U. S. A. 106, 5639–5644.
Jin, K., Tian, Y., Erickson, J.S., Puthoff, J., Autumn, K., Pesika, N., 2012. The design and fabrication of gecko-inspired adhesives. Langmuir 28, 5737.
Kendall, K., 1975. Thin-film peeling – elastic term. J. Phys. D Appl. Phys. 8, 1449–1452.
Lee, J., Fearing, R.S., Komvopoulos, K., 2008. Directional adhesion of gecko-inspired angled microfiber arrays. Appl. Phys. Lett. 93, 191910.
Murphy, M.P., Aksak, B., Sitti, M., 2009. Gecko-inspired directional and controllable adhesion. Small 5, 170–175.
Peng, Z.L., Chen, S.H., Soh, A.K., 2010. Peeling behavior of a bio-inspired nano-film on a substrate. Int. J. Solids Struct. 47, 1952–1964.
Pesika, N.S., Tian, Y., Zhao, B., Rosenberg, K., Zeng, H., McGuiggan, P., Autumn, K., Israelachvili, J.N., 2007. Peel-zone model of tape peeling based on the gecko adhesive system. J. Adhes. 83, 383–401.
Rivlin, R.S., 1944. The effective work of adhesion. Paint Technol. 9, 215–216.
Sauer, R.A., 2009. Multiscale modelling and simulation of the deformation and adhesion of a single gecko seta. Comput. Methods Biomech. 12, 627–640.
Tian, Y., Pesika, N., Zeng, H., Rosenberg, K., Zhao, B., McGuiggan, P., Autumn, K., Israelachvili, J., 2006. Adhesion and friction in gecko toe attachment and detachment. Proc. Nat. Acad. Sci. U. S. A. 103, 19320–19325.
Varenberg, M., Pugno, N.M., Gorb, S.N., 2010. Spatulate structures in biological fibrillar adhesion. Soft Matter 6, 3269–3272.
Yao, H., 2013. A generalized model for adhesive contact between a rigid cylinder and a transversely isotropic substrate. J. Appl. Mech. 80, 1027.
Yao, H., Gao, H., 2006. Mechanics of robust and releasable adhesion in biology: bottom-up designed hierarchical structures of gecko. J. Mech. Phys. Solids 54, 1120–1146.
Yao, H., Gao, H., 2009. Effects of interfacial friction on flaw tolerant adhesion between two dissimilar elastic solids. Int. J. Solids Struct. 46, 860–870.
Yu, J., Chary, S., Das, S., Tamelier, J., Pesika, N.S., Turner, K.L., Israelachvili, J.N., 2011. Gecko-inspired dry adhesive for robotic applications. Adv. Funct. Mater. 21, 3010–3018.
Zhao, B., Pesika, N., Rosenberg, K., Tian, Y., Zeng, H., McGuiggan, P., Autumn, K., Israelachvili, J., 2008. Adhesion and friction force coupling of gecko setal arrays: implications for structured adhesive surfaces. Langmuir 24, 1517–1524.